

OmniCount: Multi-label Object Counting with Semantic-Geometric Priors

Anindya Mondal^{1*}, Sauradip Nag^{2*}, Xiatian Zhu¹, Anjan Dutta¹

¹University of Surrey ²Simon Fraser University

{a.mondal, xiatian.zhu, anjan.dutta}@surrey.ac.uk, snag@sfu.ca

Abstract

Object counting is pivotal for understanding the composition of scenes. Previously, this task was dominated by class-specific methods, which have gradually evolved into more adaptable class-agnostic strategies. However, these strategies come with their own set of limitations, such as the need for manual exemplar input and multiple passes for multiple categories, resulting in significant inefficiencies. This paper introduces a more practical approach enabling simultaneous counting of multiple object categories using an open-vocabulary framework. Our solution, OmniCount, stands out by using semantic and geometric insights (priors) from pre-trained models to count multiple categories of objects as specified by users, all without additional training. OmniCount distinguishes itself by generating precise object masks and leveraging varied interactive prompts via the Segment Anything Model for efficient counting. To evaluate OmniCount, we created the OmniCount-191 benchmark, a first-of-its-kind dataset with multi-label object counts, including points, bounding boxes, and VQA annotations. Our comprehensive evaluation in OmniCount-191, alongside other leading benchmarks, demonstrates OmniCount’s exceptional performance, significantly outpacing existing solutions. The project webpage is available at <https://mondalanindya.github.io/OmniCount>.

Introduction

Understanding object distribution across multiple categories is crucial for comprehensive scene analysis, driving increased interest in object counting research. It aims to estimate specific object counts in natural scenes. Traditionally, object counting has focused on class-specific methods for categories like human crowds (Li, Zhang, and Chen 2018; Song et al. 2021; Han et al. 2023; Li et al. 2023; Liang et al. 2023; Liu et al. 2023a), cells (Khan 2016), fruits (Rahemounfar and Sheppard 2017), and vehicles (Bui, Yi, and Cho 2020). However, these methods require extensive training data and are limited to predefined categories. Recent efforts have shifted towards class-agnostic counting, using exemplars (cropped images and class names) to count arbitrary categories (Chattopadhyay et al. 2017; Ranjan et al. 2021; Ranjan and Nguyen 2022; Jiang, Liu, and Chen 2023).

*Authors have equal contributions.

Some operate in low-shot settings (You et al. 2022; Xu et al. 2023a), but they still require substantial training data and separate processing for each category, increasing computational demands for multi-category scenes. Further, detection and instance segmentation methods (Chattopadhyay et al. 2017; Cholakkal et al. 2022) can count multiple categories by name, but struggle with small or non-atomic objects like grapes or bananas, which are hard to detect individually.

Inspired by these observations, we introduce **OmniCount**, a novel method for efficiently counting multiple open-vocabulary object categories simultaneously in a single forward pass. Unlike prior zero-shot object counting (Xu et al. 2023a; Dai, Liu, and Cheung 2024) requiring substantial training on labelled seen categories, this proposed open-vocabulary object counting method leverages vision-language models to count objects across a broad spectrum of categories without any training (*i.e.*, training-free). OmniCount distinguishes itself by utilizing semantic and geometric cues from pre-trained foundation models to partition images into semantically coherent regions, identify occluded objects with depth cues, and ensure precise object delineation. A key feature is its use of geometric cues for object recovery and reducing overcounting. In general, segmentation models typically struggle with dense scenarios, leading to hallucination effects where distant or occluded objects get missed (Xie et al. 2022; Phillion and Fidler 2020). Extracting semantic and geometric priors separately helps us achieve the best of both domains. Specifically, our model uses metric depth for rectifying dense scenes where semantic estimation fails. By performing k -nearest neighbors-based searches, we refine or even recover overlooked instances, utilizing recovered object features to estimate reference points per class, enabling the counting model to handle similar-looking objects (see Fig. 4). This enables the detection of objects of varying shapes, sizes, and densities, facilitating leveraging segmentation models like the Segment Anything Model (SAM) (Kirillov et al. 2023) to generate individual object masks. SAM’s ability to use points as segmentation prompts for fine-grained, non-atomic object segmentation makes it our preferred module for counting.

As an under-studied area, object counting lacks a dataset with a diverse range of annotations for multiple generic categories per image. The sparsely populated object detection datasets like PASCAL VOC (Everingham et al. 2009)

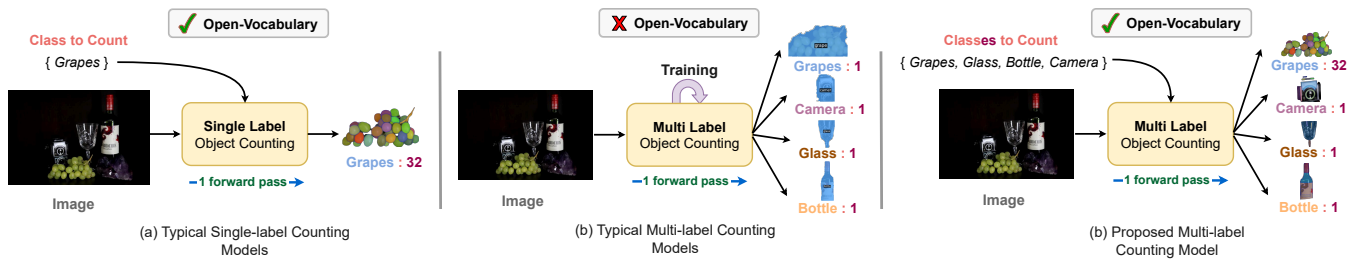


Figure 1: **Object counting paradigms:** (a) Typical single-label object counting models support open-vocabulary counting but processes only *a single category* one time. (b) Existing multi-label object counting models are training-based (i.e., not open-vocabulary) approaches and also fail to count *non-atomic objects* (e.g., grapes). (c) We advocate more efficient and convenient *multi-label open-vocabulary counting* that is training-free, and supports counting all the target categories in a single pass.

and MS COCO (Lin et al. 2014) cannot adequately represent real-world counting challenges. Additionally, the recently proposed REC-8K dataset (Dai, Liu, and Cheung 2024) focuses on fine-grained counting, distinguishing objects within the same category, like “red apples” vs. “green apples” but it doesn’t support counting across different coarse-grained categories. The absence of a suitable dataset for this underexplored domain prompted the creation of the **OmniCount-191** benchmark. This comprehensive dataset includes 302,300 object instances across 191 categories in 30,230 images, featuring multiple categories per image and a variety of detailed annotations such as counts, points and bounding boxes for each object (Fig. 5).

We make the following contributions: (1) We re-promote multi-label object counting that bypasses the conventional reliance on object detection and semantic segmentation models, addressing common accuracy issues such as over- and under-counting; (2) We introduce a novel, efficient, and user-friendly framework **OmniCount** for multi-label object counting by leveraging semantic and geometric cues without necessitating additional training; (3) We create a new multi-label object counting dataset, **OmniCount-191**, with rich annotations for fostering the development of this newly introduced setting; (4) We conduct extensive experiments to demonstrate OmniCount’s superior performance over existing methods on our dataset and establish benchmarks.

Related Work

Learning-based object counting: Traditional counting methods have focused on specific categories like crowds (Li, Zhang, and Chen 2018; Song et al. 2021; Han et al. 2023; Huang et al. 2023; Liang et al. 2023; Liu et al. 2023a; Peng and Chan 2024; Guo et al. 2024), cells (Khan 2016), fruits (Rahneemoonfar and Sheppard 2017), and vehicles (Bui, Yi, and Cho 2020), mainly using regression-based techniques to create density maps from point annotations (Lempitsky and Zisserman 2010; Zhang et al. 2016; Xu et al. 2021). These methods rely on point annotations to generate density maps, which train models that predict object counts by summing pixel values in the predicted density map. This class-specific approach is effective for its trained categories but lacks the flexibility for broader applications involving multiple object categories. In contrast, class-agnostic counting aims for versatility, using exemplars to count objects of any category (Lu, Xie, and Zisserman 2019; Zhang et al. 2019; Ranjan

et al. 2021; Shi et al. 2022; Gupta et al. 2021; Zhang et al. 2021; Ranjan and Nguyen 2022; Shi, Mettes, and Snok 2024). Some data-efficient variants operate in zero-shot (Xu et al. 2023a; Xu, Le, and Samaras 2023; Jiang, Liu, and Chen 2023; Dai, Liu, and Cheung 2024) and few-shot (You et al. 2022; Yang et al. 2021) settings, trained on seen or base classes to handle unseen or novel categories. These methods use similarity maps for flexible counting across classes, but learning-based models require extensive data, making them difficult to scale. We propose an open-vocabulary object counter that counts using prompts like points, boxes, or text, eliminating the need for training and expanding possibilities for diverse scenarios without the data and training burden.

Multi-label object counting: Despite the advancements in single-label counting, real-world scenarios often involve scenes with multiple object classes coexisting (You et al. 2022). Prior works by (Cholakkal et al. 2019, 2022) and (Chattopadhyay et al. 2017) have explored multi-label counting in sparse settings, focusing on global counts and labels within human discernible ranges. However, these methods struggle to identify non-atomic or densely clustered objects, such as grapes. Few-shot counting (Ranjan et al. 2021) attempts to address these but typically restricts to one category per image. Recently, (Dai, Liu, and Cheung 2024) introduced GrREC, a model for counting multiple fine-grained categories, but it requires training in predefined seen categories. They also developed the REC-8K dataset with images and corresponding referring expressions. In contrast, our open-vocabulary model uses semantic and geometric cues from pre-trained models without additional training. Moreover, we emphasize the need for datasets capturing real-world use cases and dense, multi-class interactions, leading to the creation of OmniCount-191.

Prompt-based foundation models: LLMs like GPT (Brown et al. 2020) have transformed NLP and computer vision, excelling in zero-shot and few-shot tasks. Foundation models like CLIP (Radford et al. 2021) use contrastive learning to align text and image, enabling effective low-shot transfer through textual prompts. In image segmentation, the Segment Anything Model (SAM) (Kirillov et al. 2023) generates precise object masks from diverse prompts (points, boxes, text), excelling in various benchmarks and showcasing robust zero-shot abilities. An ideal object counter should be *visually promptable*, *interactive*, and capable of *open-set* counting. While SAM possesses these traits, it strug-

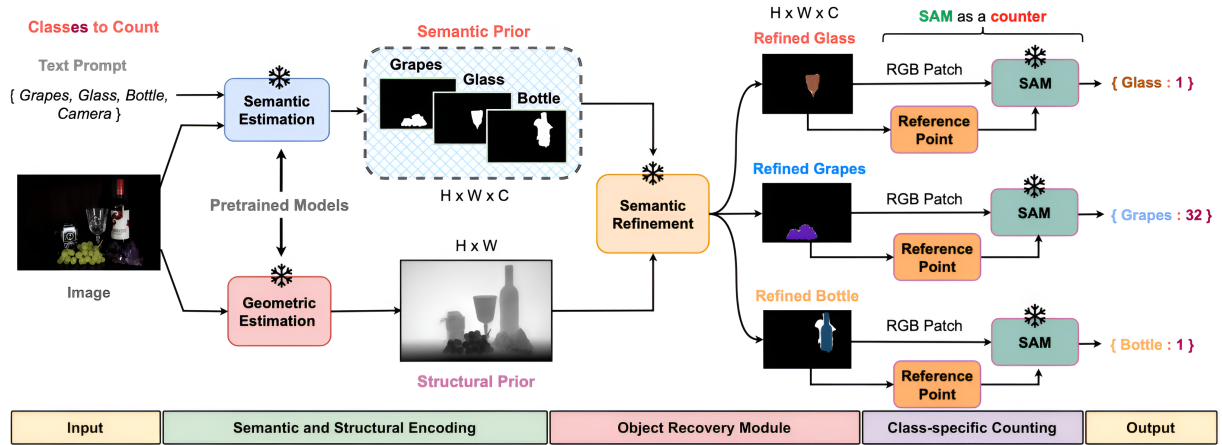


Figure 2: **OmniCount pipeline**: OmniCount processes the input image and target object classes using Semantic Estimation (SAN) and Geometric Estimation (Marigold) modules to generate class-specific masks and depth maps. These initial semantic and geometric priors are then refined through an Object Recovery module, producing precise binary masks. The refined masks help extract RGB patches and reference points, reducing over-counting. SAM then uses these RGB patches and reference points to generate instance-level masks, resulting in accurate object counts. (✳ denotes pre-trained, frozen models)

gles with occlusions (Ji et al. 2023) and multi-class object counting (Shi, Sun, and Zhang 2024) due to its class-agnostic approach. We address these challenges by incorporating depth and semantic priors into SAM, enhancing its effectiveness for complex counting tasks involving occlusions and multiple object classes, thus approaching the ideal counting model.

OmniCount

In this work, we aim to achieve open-vocabulary, multi-label training-free object counting within a given image and with a set of labels to be counted in that image. Our proposed model is illustrated in Fig. 2.

Problem formulation

The problem of multi-label object counting can be defined as obtaining an object counter $\mathcal{F}_{\text{count}}$ using a training set $\mathcal{D}_{\text{train}} = \{(I_1, \mathcal{P}_1, \mathcal{C}_1), \dots, (I_N, \mathcal{P}_N, \mathcal{C}_N)\}$, where each $I_i \in \mathbb{R}^{H \times W \times 3}$ represents an RGB image, $\mathcal{P}_i = \{p_1, \dots, p_{m_i}\}$ is a set of class labels and $\mathcal{C}_i = \{c_1, \dots, c_{m_i}\}$ are the corresponding object counts (i.e. object with label p_k occurs c_k times in I_i), with m_i being the number of unique objects in the i -th image and N the total number of training data points in $\mathcal{D}_{\text{train}}$. For an image I_k and a subset of labels $\{p_1, \dots, p_{k_l}\} \subseteq \mathcal{P}_k$, the function $\mathcal{F}_{\text{count}}$ should result in:

$$\{c_1, \dots, c_{k_l}\} = \mathcal{F}_{\text{count}}(I_k, \{p_1, \dots, p_{k_l}\}) \quad (1)$$

where c_{k_l} is the number of occurrences of the object with label p_{k_l} in the image I_k . Our goal is to develop an open-vocabulary multi-label object counting model $\mathcal{F}_{\text{count}}$, such that it generalizes well to $\mathcal{D}_{\text{test}}$, a held-out test set of data points with classes not in $\mathcal{D}_{\text{train}}$, i.e., $\mathcal{D}_{\text{train}} \cap \mathcal{D}_{\text{test}} = \phi$. To achieve this, we introduce OmniCount, a multi-label object counting model that utilizes semantic and geometric priors, avoiding training that requires large datasets and expensive computational resources. Since our model is training-free, we do not use $\mathcal{D}_{\text{train}}$ and only evaluate our model on $\mathcal{D}_{\text{test}}$.

Semantic and structural encoding

Semantic estimation module: To count multiple objects in a single forward pass, we segment the image into relevant semantic regions. While any standard open-vocabulary segmentation model can be used, we employ the Side Adapter Network (SAN) (Xu et al. 2023b) as a semantic segmentation model \mathcal{E}_{sem} that takes an image I and a set of class labels $\mathcal{P} = \{p_1, \dots, p_m\}$ as input and results in $\mathbf{S}_{\mathcal{P}} = \{S_1, \dots, S_m\}$, a set of binary semantic masks corresponding to the classes in \mathcal{P} as follows:

$$\mathbf{S}_{\mathcal{P}}, F_{\mathcal{P}} = \mathcal{E}_{\text{sem}}(I, \mathcal{P}) \quad (2)$$

where $F_{\mathcal{P}} \in \mathbb{R}^{\frac{H}{K} \times \frac{W}{K} \times C}$ is an intermediate low-resolution feature activations, with K and C being integers depending on the design of \mathcal{E}_{sem} . We use $\mathbf{S}_{\mathcal{P}}$ as a semantic prior, bridging the gap between multi-label counting and semantic awareness. While segmenting 2D RGB images, SAM (Kirillov et al. 2023) primarily relies on texture information, such as colour. Combined with occlusion, this reliance can result in over-segmented masks (see Fig. 2 for the ‘‘bottle’’ class) and, consequently, over-counting. To address this, we incorporate geometric information to achieve fine-grained segmentation, mitigating over-segmentation and over-counting. We refine the segmentation mask using geometric priors to be discussed in the next paragraph.

Geometric estimation module: Classical segmentation models (Long, Shelhamer, and Darrell 2015; Kirillov et al. 2023) primarily rely on texture information for object delineation, which often fails under significant occlusion. So, counting dense interacting or overlapping objects requires information beyond RGB. Therefore, similar to how density maps have been utilized in classical object counting by providing a clearer representation of object distribution, we leverage depth maps to enhance segmentation accuracy. Depth maps, like density maps, ignore texture and focus on structural information, aiding in the segmentation of objects regardless of their distance from the camera, as shown in Fig. 2. This structural prior helps recover hidden objects and refine object semantics. Using an off-the-shelf depth map

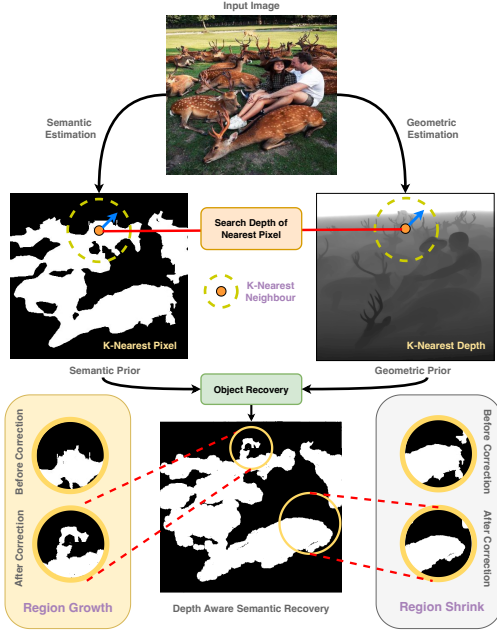


Figure 3: **Geometry aware Object Recovery:** We refine semantic masks with geometric priors using k-nearest neighbor searches to filter edge pixels by category uniqueness and depth alignment, enhancing mask precision through depth-integrated segmentation.

rendering model Marigold (Ke et al. 2024) denoted by $\mathcal{E}_{\text{depth}}$, we generate depth map D for the image I as $D = \mathcal{E}_{\text{depth}}(I)$, which serve as geometric prior for our model. Notably, D is a matrix of the same spatial dimension as the image I , with pixels having normalized depth values in $[0, 1]$. This implies that for a pixel $x \in I$, $D(x) \in [0, 1]$ indicates the normalized depth value of x . We utilize this pixel-wise depth information to refine the coarse segmentation mask $\mathbf{S}_{\mathcal{P}}$, discussed in the following subsection.

Geometry aware object recovery

Providing precise reference points is crucial for guiding SAM towards accurate counting and minimizing overcounting. We inject geometric priors into semantic priors before passing them into SAM (see Fig. 4) to obtain such reference points. To refine the semantic prior $\mathbf{S}_{\mathcal{P}}$ with geometric insights from the depth prior D , we conduct a k-nearest neighbor (kNN) (refer to Fig. 3) search centering around each of the pixels of the individual semantic mask to ensure two conditions are met:

(1) A pixel must exclusively belong to its designated object category, preventing any overlapping with masks of other categories. For a pixel x in mask S_j :

$$C_1(x) : x \notin S_k, \forall k \neq j$$

(2) The absolute difference between a pixel’s depth and the mean depth of its object category must fall below a specified tolerance τ , ensuring depth consistency (for objects with curved edges). For a pixel x in S_n with mean depth $D_{\mu}(S_n)$:

$$C_2(x) : |D(x) - D_{\mu}(S_n)| < \tau$$

where $D(x)$ denotes the depth of pixel x and $D_{\mu}(S_n) = \frac{1}{s} \sum_y D(y), \forall y \in S_n$ with s as the total number of pixels in

S_n . Pixels that fulfil both conditions $C_1(x)$ and $C_2(x)$ are integrated into their appropriate object class, leading to a refined semantic prior $\mathbf{S}'_{\mathcal{P}}$, computed as $\mathbf{S}'_{\mathcal{P}} = \mathcal{R}_{\text{geom}}(\mathbf{S}_{\mathcal{P}}, D)$, where $\mathcal{R}_{\text{geom}}$ is the geometry-aware semantic refinement function, enhancing the precision of semantic masks by considering depth information. This depth-aware refined mask (see Fig. 3) minimizes the risk of over-segmentation (see Table 3) or recovers undiscovered objects in occluded scenes.

Reference point guided counting

We use SAM (Kirillov et al. 2023) as an object counter, which employs a point grid generator to place uniform points across the image and generate masks. This can lead to overcounting due to points falling on both foreground and background. To prevent this, we propose a reference point selection procedure that focuses solely on the foreground.

Reference point selection: We select reference points (refer to Fig. 4) for the SAM decoder using the feature activation $F_{\mathcal{P}}$ from semantic priors (see Eq. (2)) to enhance text-image similarity accuracy. A set of reference points $\mathbf{P} = \{\rho_1, \dots, \rho_s\}$ are identified as local maxima within $F_{\mathcal{P}}$, but direct upsampling can misalign (Zhang et al. 2020) them due to quantization errors (refer to Table 3). To address this, we apply Gaussian refinement to the low-resolution reference points \mathbf{P} (Zhang et al. 2020), resulting in corrected reference points $\mathbf{P}' = \{\rho'_1, \dots, \rho'_s\}$. To specifically target foreground objects and avoid background segmentation, we compute the Hadamard product between the refined semantic mask S'_m for class p_m and the corrected reference points \mathbf{P}' as $\mathbf{Q}_m = S'_m \circ \mathbf{P}'$, where \circ represents the Hadamard product, and $\mathbf{Q}_m \subseteq \mathbf{P}'$ denotes the set of resulting reference points for objects belonging to the label p_m , serving as a guide for identifying regions likely to contain the target objects, as illustrated in Fig. 4. This ensures the reference points \mathbf{Q}_m to guide the segmentation to the target objects. These per-class reference points act as density maps (see Fig. 9(b)), allowing for accurate object counting across varying densities. This automated selection can also be replaced by manual point or box annotations, making our model interactive for multiple user inputs.

SAM mask generator: By incorporating the reference object activation $F_{\mathcal{P}}$ and modifying the mask generation process, SAM’s mask decoder can better focus on the reference object features. This additional contextual information from $F_{\mathcal{P}}$ helps the mask generator accurately distinguish and segment target objects. Since SAM’s encoder requires an RGB image, we extract an RGB patch I_m of the target object by multiplying the input image I with the refined semantic mask S'_m (see Fig. 3). The resultant mask \mathbf{M}_m from SAM is obtained as $\mathbf{M}_m = \text{SAM}(I_m, \mathbf{Q}_m)$, where $\mathbf{M}_m = \{M_{m_1}, \dots, M_{m_n}\}$ is the set of individual object masks segmented by SAM. We count these masks to determine the total number of objects for class label p_m . This approach focuses on target objects without segmenting unrelated entities, enhancing efficiency and accuracy beyond the standard “segment everything” strategy. Finally, masks that are empty or cover an insignificantly small area are discarded, creating a refined subset $\mathbf{N}_m \subseteq \mathbf{M}_m$ containing only significant masks for the final object count. The cardi-

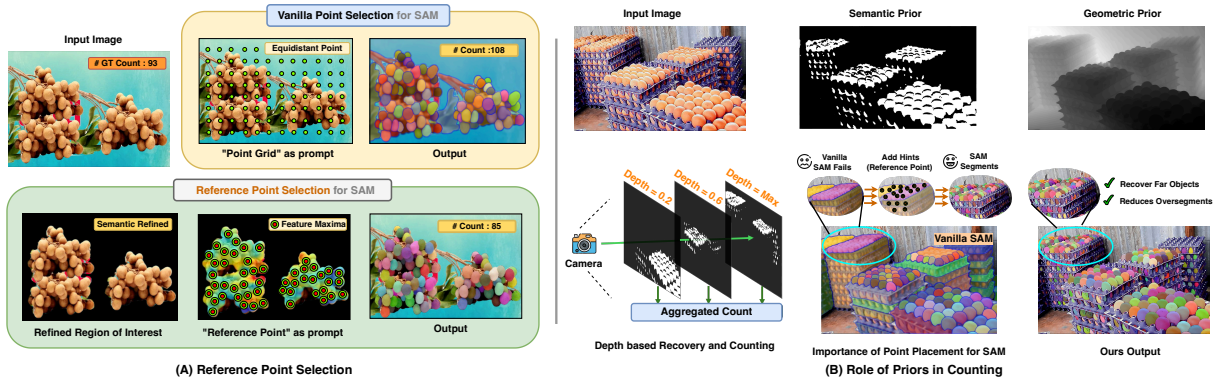


Figure 4: **Reference Point Selection:** SAM’s segmentation accuracy is enhanced by refining reference point selection. Panel (A) shows how integrating semantic priors, identifying local maxima, and applying Gaussian refinement improve reference point accuracy, focusing them on foreground objects for better segmentation and counting. Panel (B) demonstrates the benefits of incorporating semantic and geometric priors, where depth-based recovery and precise reference points help SAM recover distant or occluded objects, reducing over-segmentation issues found in the default “everything mode”.

nality of N_m , $\text{card}(N_m)$, denotes the final count of objects of class-label m in image I .

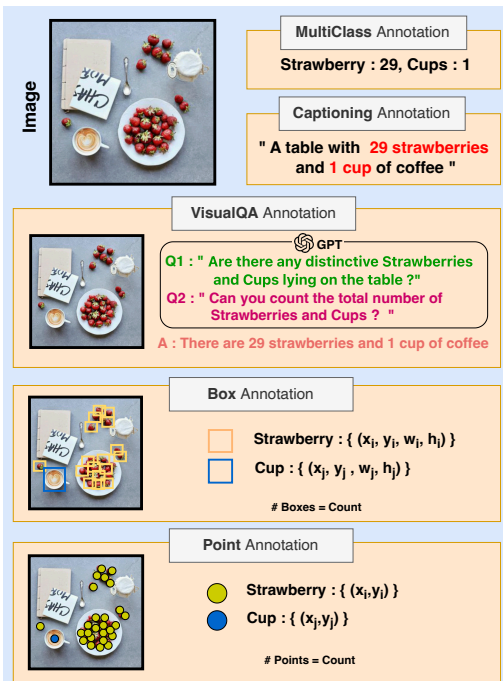


Figure 5: **OmniCount-191 Annotations:** A collection of images with 191 classes across nine domains, annotating each image with captions, VQA, boxes, and points.

OmniCount-191 Dataset

To effectively evaluate OmniCount across open-vocabulary, supervised, and few-shot counting tasks, a dataset catering to a broad spectrum of visual categories and instances featuring various visual categories with multiple instances and classes per image is essential. The current datasets, primarily designed for object counting (Ranjan et al. 2021) focusing on singular object categories like humans and vehicles, fall short for multi-label object counting tasks. Despite the presence of multi-class datasets like MS COCO (Lin et al.

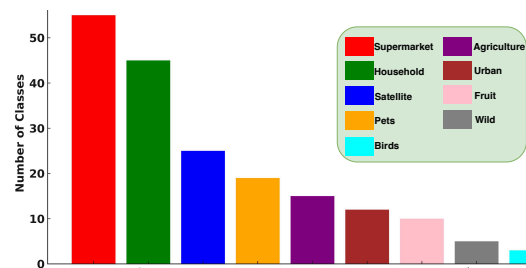


Figure 6: **OmniCount-191 statistics:** The number of categories per domain in long-tailed distribution format.

2014), PASCAL VOC (Everingham et al. 2009), and REC-8K (Dai, Liu, and Cheung 2024), their utility is limited for counting due to the sparse nature of object appearance and fine-grained referencing. Addressing this gap, we created a new dataset with 30,230 images spanning 191 diverse categories, including kitchen utensils, office supplies, vehicles, and animals. This dataset features a wide range of object instance counts per image, ranging from 1 to 160, with an average of 10, bridging the existing gap and setting a benchmark for assessing counting models in varied scenarios.

Dataset statistics: The OmniCount-191 benchmark presents images with small, densely packed objects from multiple classes, reflecting real-world object counting scenarios. This dataset encompasses 30,230 images, with dimensions averaging 700×580 pixels. Each image contains an average of 10 objects, totalling 302,300, with individual images ranging from 1 to 160. We use the same annotation rules defined in existing counting datasets (Ranjan et al. 2021). To ensure diversity, the dataset is split into training and testing sets, with no overlap in object categories – 118 categories for training and 73 for testing, corresponding to a 60%-40% split. This results in 26,978 images for training and 3,252 for testing. Class splits are available for few and zero-shot settings for specific applications, detailed in the supplementary.

Experiments

Datasets: For multi-label counting, we evaluate OmniCount on our proposed OmniCount-191 benchmark, specifically designed for multi-class scenarios. Additionally, following

| Methods | Training | PASCAL VOC | | OmniCount-191 | |
|------------------------------|----------|---------------|--------------|---------------|-------------|
| | | mRMSE ↓ | mRMSE-nz ↓ | mRMSE ↓ | mRMSE-nz ↓ |
| ILC (Cholakkal et al.) | ✓ | 0.29 | 1.14 | 4.56 | 9.39 |
| CEOES (Chattopadhyay et al.) | ✓ | 0.42 | 1.65 | - | - |
| Grounding-DINO (Liu et al.) | ✗ | 0.0066 | 0.05 | 1.29 | 3.27 |
| CLIPSeg (Lüdtke and Ecker) | ✗ | 0.0091 | 0.08 | 1.54 | 4.28 |
| TFOC (Shi, Sun, and Zhang) | ✗ | 0.0084 | 0.03 | 0.95 | 2.89 |
| GrREC (Dai, Liu, and Cheung) | ✓ | - | - | <u>0.50</u> | <u>1.87</u> |
| OmniCount | ✗ | 0.0023 | 0.009 | 0.70 | 2.00 |

Table 1: **Performance comparison in multi-label object counting using text prompts.** Results on the PASCAL VOC and OmniCount-191 datasets. Methods requiring training are marked (✓). The best results are in **bold**, while the best scores among the learning-based methods are underlined. Zero-shot models are marked **blue**.

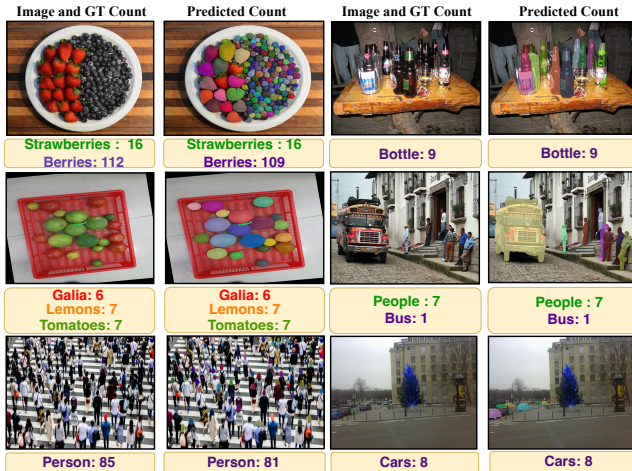


Figure 7: **Qualitative Results using OmniCount:** OmniCount-191 (left), PASCAL VOC (right).

the detection and segmentation-based models (Chattopadhyay et al. 2017) for multi-label counting, we compare OmniCount on the PASCAL VOC dataset (Everingham et al. 2009), which includes 9963 images across 20 real-world classes, with 4952 designated for testing. For single-class counting, we used the test sets from FSC-147 (Ranjan et al. 2021) and CARPK (Hsieh, Lin, and Hsu 2017). Among them, FSC-147 includes 1190 images across 29 categories, while CARPK provides 1014 test images. FSC-147 and CARPK offer point and box annotations compatible with our model, whereas PASCAL VOC only provides box annotations.

Multi-label object counting

Competitors: For a fair comparison with state-of-the-art methods, we adapt the single-label object counting model TFOC (Shi, Sun, and Zhang 2024) for multi-label counting by running it for each class in an image to obtain multi-label counts. We also replicate and evaluate the performance of ILC (Cholakkal et al. 2019) and GrREC (Dai, Liu, and Cheung 2024) for a direct comparison, though replicating CEOES (Chattopadhyay et al. 2017) was limited by its Lua implementation. We additionally employ open-vocabulary object detection (Grounding-DINO (Liu et al. 2023b)) and semantic segmentation (CLIPSeg (Lüdtke and Ecker 2022)) baselines for multi-label counting. The Grounding-DINO baseline counts objects by enumerating detected bounding boxes per category, while the CLIPSeg

baseline uses a ViT encoder and spectral clustering to estimate category counts by identifying connected components. **Results:** In Table 1, we compare OmniCount with existing multi-label counting methods, demonstrating its strong performance, especially as a training-free model. Although the recently introduced GrREC, a training-based method, achieves slightly better scores, OmniCount remains highly competitive despite not being trained on seen classes. This highlights the benefits of our open-vocabulary approach, which uses geometric priors to accurately count multiple categories in a single pass – unlike traditional models that struggle with occlusions and require separate passes for each category. Notably, our SAM-based OmniCount surpasses the CLIPSeg and Grounding-DINO baselines, confirming SAM’s effectiveness for counting tasks. Qualitative results in Fig. 7 show OmniCount’s performance on OmniCount-191 and PASCAL VOC, while Fig. 8 compares it with TFOC on OmniCount-191. These results highlight OmniCount’s robustness in counting objects of various sizes, from large singular items like seals and buses to medium-sized objects (e.g. bottles, cars etc.) and small, non-atomic entities like pulses and berries. Further analysis using ground-truth bounding box and point annotations is provided in the supplementary material.

Single-label counting

Competitors: We report the performance of training-based methods like CFOCNet+ (Yang et al. 2021), GMN (Lu, Xie, and Zisserman 2019), BMNet (Shi et al. 2022), ZSOC (Xu et al. 2023a), PSeCo (Huang 2024), GrREC (Dai, Liu, and Cheung 2024), as well as training-free approaches like TFOC (Shi, Sun, and Zhang 2024). We have also adopted a SAM-based baseline for a fair comparison, reporting Vanilla SAM (Kirillov et al. 2023) counting results by processing entire images with a uniform point layout.

Results: We rigorously compare our model’s performance in a single-label context utilizing text, box, and point prompts, as shown in Table 2. Like multi-label counting, OmniCount consistently outperforms major training-based models, and all training-free models across all the text/box/point prompt modalities across four key metrics demonstrate its robustness and efficiency in object counting tasks. This also illustrates that merely using SAM as a counting model is inferior, even in single-class counting, highlighting the importance of different priors. More results and insights on other OmniCount-191 tasks, such as VQA, have been provided in the supplementary material.

Further analysis

Impact of depth refinement: OmniCount leverages semantic (SP) and geometric priors (GP) to improve SAM’s segmentation performance, making it suitable as an object counter. We assess the impact of SP and GP on SAM’s object counting performance using the OmniCount-191 dataset, as shown in Table 3. The best results (rows 2-4) indicate that without GP, OmniCount has 56/8% higher error rate in m-RMSE/m-RMSE-nz metrics, suggesting that SAM over-segments and over-counts when it lacks structural/geometric information for occluded objects.

| Models | Training | Prompt | FSC-147 | | | | CARPK | | | |
|------------------------------------|----------|--------|--------------|---------------|-------------|-------------|--------------|--------------|-------------|-------------|
| | | | MAE ↓ | RMSE ↓ | NAE ↓ | SRE ↓ | MAE ↓ | RMSE ↓ | NAE ↓ | SRE ↓ |
| CFOCNet+ (Yang et al. 2021) | ✓ | box | 22.10 | 112.71 | - | - | - | - | - | - |
| GMN (Lu, Xie, and Zisserman 2019) | ✓ | box | 26.52 | 124.57 | - | -7.48 | 9.90 | - | - | - |
| BMNet+ (Shi et al. 2022) | ✓ | box | <u>14.62</u> | 91.83 | <u>0.25</u> | <u>2.74</u> | <u>5.76</u> | <u>7.83</u> | - | - |
| Vanilla SAM (Kirillov et al. 2023) | ✗ | N.A. | 42.48 | 137.50 | 1.14 | 8.13 | 16.97 | 20.57 | 0.70 | 5.30 |
| PSeCo (Huang 2024) | ✓ | N.A. | 16.58 | 129.77 | - | - | - | - | - | - |
| TFOC (Shi, Sun, and Zhang 2024) | ✗ | box | 19.95 | 132.16 | 0.29 | 3.80 | 10.97 | 14.24 | 0.48 | 3.70 |
| OmniCount | ✗ | box | 18.63 | 112.98 | 0.14 | 2.99 | 9.92 | 12.15 | 0.23 | 2.11 |
| TFOC (Shi, Sun, and Zhang 2024) | ✗ | point | 20.10 | 132.83 | 0.30 | 3.87 | 11.01 | 14.34 | 0.51 | 3.89 |
| OmniCount | ✗ | point | 19.24 | 115.27 | 0.25 | 3.21 | 10.66 | 13.15 | 0.31 | 2.45 |
| ZSOC (Xu et al. 2023a) | ✓ | text | 22.09 | 115.17 | 0.34 | 3.74 | - | - | - | - |
| TFOC (Shi, Sun, and Zhang 2024) | ✗ | text | 24.79 | 137.15 | 0.37 | 4.52 | - | - | - | - |
| GrREC (Dai, Liu, and Cheung 2024) | ✓ | text | <u>10.12</u> | <u>107.19</u> | - | - | - | - | - | - |
| OmniCount | ✗ | text | 21.46 | 133.28 | 0.32 | 0.39 | - | - | - | - |

Table 2: Results in single-label object counting setting using text, point, and box prompts. The **bold** denotes the best among training-free methods, while the underlined font is the best among learning-based methods. Zero-shot models are marked **blue**.

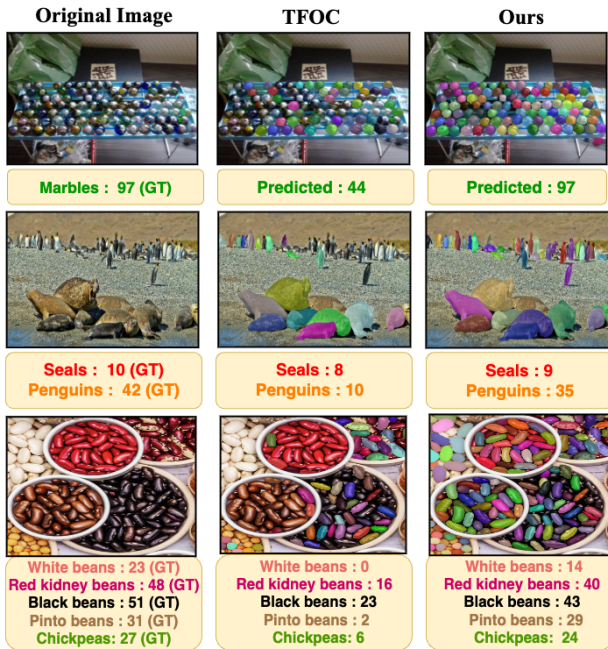


Figure 8: Qualitative comparisons with TFOC on the OmniCount-191 dataset.

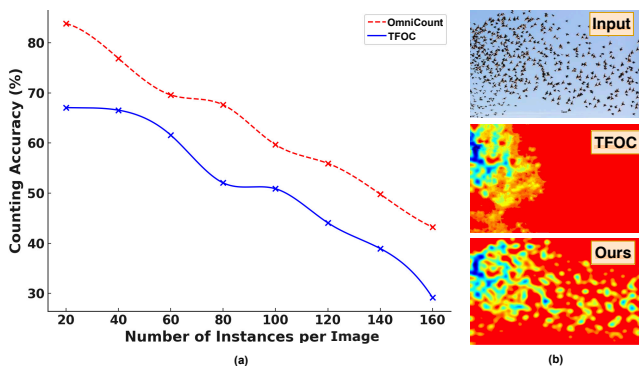


Figure 9: Performance comparison in dense scenes. (a) Counting accuracy vs number of instances per image (b) Counting heatmap in varying depth image

Importance of reference points: OmniCount employs reference point (RP) selection using the feature activation

| SP | GP | RP | m-RMSE ↓ | m-RMSE-nz ↓ |
|----|----|----|-------------|-------------|
| ✓ | ✗ | ✗ | 7.02 | 5.89 |
| ✓ | ✗ | ✓ | 1.62 | 2.17 |
| ✓ | ✓ | ✗ | 2.12 | 2.54 |
| ✓ | ✓ | ✓ | 0.70 | 2.00 |

Table 3: Ablation of Semantic Prior (SP), Geometric Prior (GP) and Reference Point (RP) on OmniCount-191 dataset.

F_p from semantic priors, feeding the selected RPs into SAM for segmentation and counting. In this experiment, we have evaluated the impact of RP selection versus SAM’s default “everything mode” on object counting using the OmniCount-191 dataset, as shown in Table 3. The best results (rows 3-4) indicate that SAM’s “everything mode” with uniform point selection leads to overcounting, with a 67/21% increase in error rates, showing the effectiveness of our reference point selection step.

Counting ability in dense scenarios: In Fig. 9, we compare the counting performance of OmniCount and TFOC in dense scenes from OmniCount-191. As shown in Fig. 9(a), both models experience a decline in performance as the number of instances per image increases. This deterioration is more pronounced in TFOC due to its reliance on segmentation methods, which struggle with occlusions and dense object distributions. This also justifies why object counting approaches do not work well on crowd counting (Pelhan et al. 2024). Adding depth priors helps mitigate these errors, as reflected in OmniCount’s improved performance. Similarly, in Fig. 9(b), while TFOC can count birds close to the camera, our method can identify them at varying depths, even ones in the sky with infinite depth.

Conclusion

We introduced OmniCount, a novel open-vocabulary, multi-label counting model capable of processing multiple categories in a single pass, integrating semantic and geometric insights without requiring training. Surpassing traditional, category-specific models limited by dataset constraints, OmniCount utilizes pre-trained foundation models for semantic segmentation and depth estimation to address occlusions and achieve precise object segmentation and counting. To fill the void of a dedicated multi-label counting dataset, we developed OmniCount-191, featuring 30,230 images across 191 categories. OmniCount’s efficacy, tested on existing bench-

marks and our OmniCount-191 in various settings, showcases its superior performance, efficiency, and scalability, emphasizing its readiness for real-world applications and establishing multi-label counting as a practical, feasible tool.

References

- Brown, T.; Mann, B.; Ryder, N.; Subbiah, M.; Kaplan, J. D.; Dhariwal, P.; and et al. 2020. Language models are few-shot learners. *NeurIPS*.
- Bui, K.-H. N.; Yi, H.; and Cho, J. 2020. A Vehicle Counts by Class Framework using Distinguished Regions Tracking at Multiple Intersections. In *CVPRW*.
- Chattopadhyay, P.; Vedantam, R.; Selvaraju, R. R.; Batra, D.; and Parikh, D. 2017. Counting Everyday Objects in Everyday Scenes. In *CVPR*.
- Cholakkal, H.; Sun, G.; Khan, F. S.; and Shao, L. 2019. Object counting and instance segmentation with image-level supervision. In *CVPR*.
- Cholakkal, H.; Sun, G.; Khan, S.; Khan, F. S.; Shao, L.; and Gool, L. V. 2022. Towards Partial Supervision for Generic Object Counting in Natural Scenes. *IEEE TPAMI*.
- Dai, S.; Liu, J.; and Cheung, N.-M. 2024. Referring Expression Counting. In *CVPR*.
- Everingham, M.; Gool, L. V.; Williams, C. K. I.; Winn, J.; and Zisserman, A. 2009. The PASCAL Visual Object Classes (VOC) Challenge. *IJCV*.
- Guo, M.; Yuan, L.; Yan, Z.; Chen, B.; Wang, Y.; and Ye, Q. 2024. Regressor-Segmenter Mutual Prompt Learning for Crowd Counting. In *CVPR*.
- Gupta, S. K.; Zhang, M.; Wu, C.-C.; Wolfe, J.; and Kreiman, G. 2021. Visual search asymmetry: Deep nets and humans share similar inherent biases. In *NeurIPS*.
- Han, T.; Bai, L.; Liu, L.; and Wanli, O. 2023. STEERER: Resolving Scale Variations for Counting and Localization via Selective Inheritance Learning. In *ICCV*.
- Hsieh, M.-R.; Lin, Y.-L.; and Hsu, W. H. 2017. Drone-based object counting by spatially regularized regional proposal network. In *ICCV*.
- Huang, Z. e. a. 2024. Point Segment and Count: A Generalized Framework for Object Counting. In *CVPR*.
- Huang, Z.-K.; Chen, W.-T.; Chiang, Y.-C.; Kuo, S.-Y.; and Yang, M.-H. 2023. Counting Crowds in Bad Weather. In *ICCV*.
- Ji, G.-P.; Fan, D.-P.; Xu, P.; Cheng, M.-M.; Zhou, B.; and Van Gool, L. 2023. SAM Struggles in Concealed Scenes – Empirical Study on “Segment Anything”. *SCIS*.
- Jiang, R.; Liu, L.; and Chen, C. 2023. CLIP-Count: Towards Text-Guided Zero-Shot Object Counting. In *ACM MM*.
- Ke, B.; Obukhov, A.; Huang, S.; Metzger, N.; Daudt, R. C.; and Schindler, K. 2024. Marigold: Repurposing Diffusion-Based Image Generators for Monocular Depth Estimation. In *CVPR*.
- Khan, A. 2016. Deep Convolutional Neural Networks for Human Embryonic Cell Counting. In *ECCV*.
- Kirillov, A.; Mintun, E.; Ravi, N.; Mao, H.; Rolland, C.; Gustafson, L.; Xiao, T.; Whitehead, S.; Berg, A. C.; Lo, W.-Y.; et al. 2023. Segment anything. In *ICCV*.
- Lempitsky, V.; and Zisserman, A. 2010. Learning to count objects in images. In *NeurIPS*.
- Li, C.; Hu, X.; Abousamra, S.; and Chen, C. 2023. Calibrating Uncertainty for Semi-Supervised Crowd Counting. In *ICCV*.
- Li, Y.; Zhang, X.; and Chen, D. 2018. CSRNet: Dilated convolutional neural networks for understanding the highly congested scenes. In *CVPR*.
- Liang, D.; Xie, J.; Zou, Z.; Ye, X.; Xu, W.; and Bai, X. 2023. CrowdCLIP: Unsupervised Crowd Counting via Vision-Language Model. In *CVPR*.
- Lin, T.-Y.; Maire, M.; Belongie, S.; Hays, J.; Perona, P.; Ramanan, D.; Dollár, P.; and Zitnick, C. L. 2014. Microsoft COCO: Common objects in context. In *ECCV*.
- Liu, C.; Lu, H.; Cao, Z.; and Liu, T. 2023a. Point-Query Quadtree for Crowd Counting, Localization, and More. In *ICCV*.
- Liu, S.; Zeng, Z.; Ren, T.; Li, F.; Zhang, H.; Yang, J.; Li, C.; Yang, J.; Su, H.; Zhu, J.; et al. 2023b. Grounding DINO: Marrying DINO with Grounded Pre-Training for Open-Set Object Detection. In *ECCV*.
- Long, J.; Shelhamer, E.; and Darrell, T. 2015. Fully convolutional networks for semantic segmentation. In *CVPR*.
- Lu, E.; Xie, W.; and Zisserman, A. 2019. Class-agnostic counting. In *ACCV*.
- Lüddecke, T.; and Ecker, A. 2022. Image segmentation using text and image prompts. In *CVPR*.
- Pelhan, J.; Zavrtanik, V.; Kristan, M.; et al. 2024. DAVE - A Detect-and-Verify Paradigm for Low-Shot Counting. In *CVPR*.
- Peng, Z.; and Chan, S.-H. G. 2024. Single Domain Generalization for Crowd Counting. In *CVPR*.
- Phillion, J.; and Fidler, S. 2020. Lift, splat, shoot: Encoding images from arbitrary camera rigs by implicitly unprojecting to 3d. In *ECCV*.
- Radford, A.; Kim, J. W.; Hallacy, C.; Ramesh, A.; Goh, G.; Agarwal, S.; Sastry, G.; Askell, A.; Mishkin, P.; Clark, J.; et al. 2021. Learning transferable visual models from natural language supervision. In *ICML*.
- Rahneemoonfar, M.; and Sheppard, C. 2017. Deep Count: Fruit Counting Based on Deep Simulated Learning. In *Sensors*.
- Ranjan, V.; and Nguyen, M. H. 2022. Exemplar Free Class Agnostic Counting. In *ACCV*.
- Ranjan, V.; Sharma, U.; Nguyen, T.; and Hoai, M. 2021. Learning To Count Everything. In *CVPR*.
- Shi, M.; Lu, H.; Feng, C.; Liu, C.; and Cao, Z. 2022. Represent, compare, and learn: A similarity-aware framework for class-agnostic counting. In *CVPR*.
- Shi, Z.; Mettes, P.; and Snoek, C. G. 2024. Focus for Free in Density-Based Counting. *IJCV*.

Shi, Z.; Sun, Y.; and Zhang, M. 2024. Training-free Object Counting with Prompts. In *WACV*.

Song, Q.; Wang, C.; Jiang, Z.; Wang, Y.; Tai, Y.; Wang, C.; Li, J.; Huang, F.; and Wu, Y. 2021. Rethinking Counting and Localization in Crowds: A Purely Point-Based Framework. In *ICCV*.

Xie, E.; Yu, Z.; Zhou, D.; Phillion, J.; Anandkumar, A.; Fidler, S.; Luo, P.; and Alvarez, J. M. 2022. M2BEV: Multi-Camera Joint 3D Detection and Segmentation with Unified Bird's-Eye View Representation. *arXiv preprint*.

Xu, J.; Le, H.; Nguyen, V.; Ranjan, V.; and Samaras, D. 2023a. Zero-Shot Object Counting. In *CVPR*.

Xu, J.; Le, H.; and Samaras, D. 2023. Zero-Shot Object Counting with Language-Vision Models. *arXiv preprint arXiv:2309.13097*.

Xu, M.; Zhang, Z.; Wei, F.; Hu, H.; and Bai, X. 2023b. Side adapter network for open-vocabulary semantic segmentation. In *CVPR*.

Xu, Y.; Zhong, Z.; Lian, D.; Li, J.; Li, Z.; Xu, X.; and Gao, S. 2021. Crowd counting with partial annotations in an image. In *ICCV*.

Yang, S.-D.; Su, H.-T.; Hsu, W. H.; and Chen, W.-C. 2021. Class-agnostic few-shot object counting. In *WACV*.

You, Z.; Yang, K.; Luo, W.; Lu, X.; Cui, L.; and Le, X. 2022. Few-shot Object Counting with Similarity-Aware Feature Enhancement. In *WACV*.

Zhang, F.; Zhu, X.; Dai, H.; Ye, M.; and Zhu, C. 2020. Distribution-aware coordinate representation for human pose estimation. In *CVPR*.

Zhang, L.; Shi, Z.; Cheng, M.-M.; Liu, Y.; Bian, J.-W.; Zhou, J. T.; Zheng, G.; and Zeng, Z. 2019. Nonlinear regression via deep negative correlation learning. *IEEE TPAMI*.

Zhang, M.; Armendariz, M.; Xiao, W.; Rose, O.; Bendtz, K.; Livingstone, M.; Ponce, C.; and Kreiman, G. 2021. Look Twice: A Generalist Computational Model Predicts Return Fixations across Tasks and Species. *PLOS Comp. Bio.*

Zhang, Y.; Zhou, D.; Chen, S.; Gao, S.; and Ma, Y. 2016. Single-image crowd counting via multi-column convolutional neural network. In *CVPR*.